Journal of Sound and Vibration (1997) **204**(4), 575–584

PARAMETER ESTIMATION AND DAMPING PERFORMANCE OF ELECTRO-RHEOLOGICAL DAMPERS

G. Z. Yao, G. Meng and T. Fang

Institute of Vibration Engineering, Northwestern Polytechnical University, Xi'an 710072, *People's Republic of China*

(*Received* 29 *May* 1996, *and in final form* 30 *January* 1997)

Electro-rheological (ER) fluid is a kind of smart material with bright prospects for industrial applications. Its viscosity can be changed instantaneously by changing the intensity of an imposed electric field. In this paper two types of ER dampers, the MP one with multi-electrode plates and the SP one with sliding electrode plates, are designed. Experiments involving sinusoidal excitations and random excitations show that they are very effective in vibration control for excitation frequencies below 100 Hz, but are less or no longer effective for excitation frequencies over 100 Hz. It is the large viscous damping of the ER damper that suppresses the vibration in the lower frequency bands. However, ER fluid may change from liquid to a solid-like structure due to the high intensity of an imposed electric field, which causes the rapid rise of Coulomb frictions, but too large Coulomb friction will increase the response of the ER damper in the higher frequency bands. The MP damper has a broader varying range of damping than the SP one. Under high electric field intensity, the damping and stiffness of ER dampers change considerably, exhibiting strong non-linearity. The natural frequency of an ER damper shifts with the varying electric field due to changing stiffness. The viscous friction force and Coulomb friction force of an ER damper are estimated by a recursive least-square algorithm. The change in stiffness has been considered in the estimation. The estimated results agree very well with the experimental results.

1. INTRODUCTION

Electro-rheological (ER) fluid is a kind of smart material with variable viscosity under varying electric field intensity. When the electric field intensity reaches a threshold value, ER fluid will change from liquid to a solid-like structure, exhibiting solid-like characteristics. The change is almost instantaneous, within a few milliseconds or so, and is reversible. It means that when the electric field is removed, ER fluid will change from the solid-like structure back to liquid instantaneously. The energy consumption during this process is very little. The above mentioned characteristics of ER fluid are very useful, especially for vibration control. Up to now, many kinds of ER fluids have been discovered [1–3], and many researchers have studied the applications of ER fluid to vibration control of mechanical systems, such as vehicle suspension systems [4–6], engine mounts, and rotor systems of rotating machineries [7–10]. Many achievements were obtained in these fields [11, 12]. ER dampers may be divided into two types [13]: the FP with fixed electrode plates and the SP with sliding electrode plates. Each of these two types has its own advantages. The size of the SP damper is smaller than that of the FP damper. Usually the relative moving area of plates of the SP one is small, and so the damping produced is limited. On

0022–460X/97/290575 + 10 $25.00/0/sv970959

the other hand, the FP damper has a by-pass line with a large relative electrode area and a long flow passage. Hence, the FP damper can provide larger damping, but its dimension is larger because of the by-pass line.

Several FP dampers and SP dampers have been developed experimentally [4–6]. In Reference [14], an ER vibration damper with sliding plates was investigated experimentally and theoretically, and its parameters were estimated without considering the change of stiffness. In this paper, an MP damper with multi-electrode plates is designed. Without imposing any electric field on it, the MP damper provides very little damping. However, the MP damper can provide very large damping when an electric field is imposed on it. The varying damping range of an MP damper is very wide. Meanwhile an SP damper is also designed for comparative study. Experiments are carried out for both two dampers under sinusoidal and random excitations. Experimental results show that both dampers are very effective when the excitation frequencies are below 100 Hz, especially when the excitation frequencies are lower than 40 Hz. Both ER dampers exhibit non-linear effects under either sinusoidal or random test. The parameters of the MP damper are estimated by a non-linear parameter estimation algorithm. The change in stiffness has been considered in the estimation. Both the estimated and the experimental results show that the stiffness changes considerably and the natural frequency shifts.

2. STRUCTURES OF THE ER DAMPER AND EXPERIMENTAL ARRANGEMENT

The MP damper shown in Figure 1(a), has two positive electrode plates and two negative ones. Two of the negative electrodes and one of the positive electrodes are fixed together as a sliding part supported by a spring, moving up and down like a piston. An SP damper is designed for comparative study (see Figure 1(b)). ER fluid used in the experiment was made from transformer oil mixed with organic particles and additives, which has a maximum yield stress of 2.3 kPa at 3 kV/mm electric field intensity. The viscosity of the transformer oil used as based fluid is 20 cST at 20°C. The electrode plates are uniformly placed at a distance of $h = 2$ mm.

Experimental instrumentation for these two ER dampers is shown in Figure 2. The ER damper, together with an impedance head (B&K, Type 8001), is connected through an excitation bar, to a fixed exciter. The high voltage is supplied by a d.c. power source, which ranges from 0 to 5000 V. The signals from the impedance head are sent to SD 380 Dynamic Signal Analyzer through B&K Charge Amplifiers (Type 2635). The excitation signals are produced by the SD 380 and preamplified before being sent to the exciter.

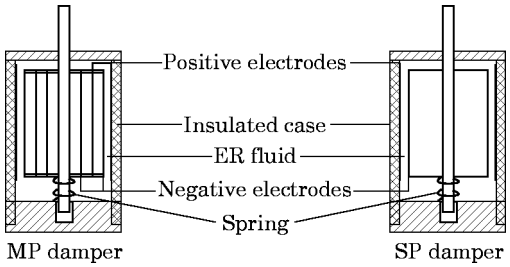

Figure 1. Structure of ER dampers.

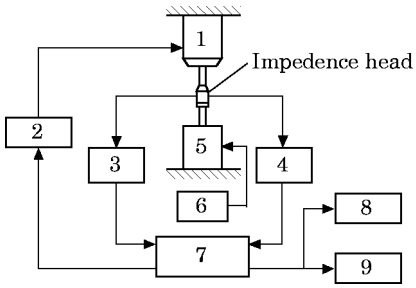

Figure 2. Experimental arrangement. 1, Exciter; 2–4, amplifier; 5, ER damper; 6, high voltage power supply; 7, SD 380 dynamic signal analyzer; 8, computer; 9, plotter.

3. EXPERIMENTAL PROCEDURES AND RESULTS DISCUSSION

Experiments were carried out at voltages of 0, 1000, 2000, 3000, 3750, 4500 and 5000 V at room temperature. The corresponding electric field intensities were 0, 0·5, 1, 1·5 1·875, 2·25 and 2·5 kV/mm, respectively.

First, experiments for an MP damper were carried out under sinusoidal excitations, from 5–120 Hz with a uniform 5 Hz step under prescribed voltages. The force and acceleration signals were sampled by the SD 380. After processing, the transfer functions were recorded or sent to a plotter. Secondly, experiments for the MP damper were carried out under swept random excitations with center frequencies from 0–400 Hz. Then, experiments for a SP damper were carried out for the same conditions, as described above.

The plots of the maximum acceleration varying with electric field intensity for a MP damper are shown in Figure 3(a), for excitation frequencies of 10, 20, 30, 40, 50 and 60 Hz, respectively. It must be emphasized that the strength of the excitation force is different for different frequencies, so comparison can only be carried out for the slopes. One can see from Figure 3(a) that the accelerations for frequencies 10, 20 and 30 Hz decrease rapidly with the increase of electric field intensity when the electric field intensity is lower than 1·5 kV/mm. The accelerations for frequencies of 10 and 20 Hz change very little when the electric field intensity is over 1·5 kV/mm. The decrease of acceleration amplitude with the increase of electric field intensity for frequencies higher than 40 Hz is very small. Experiments show that the acceleration even increases with the electric field intensity for excitation frequency greater than 100 Hz. This might be due to the increase of the Coulomb

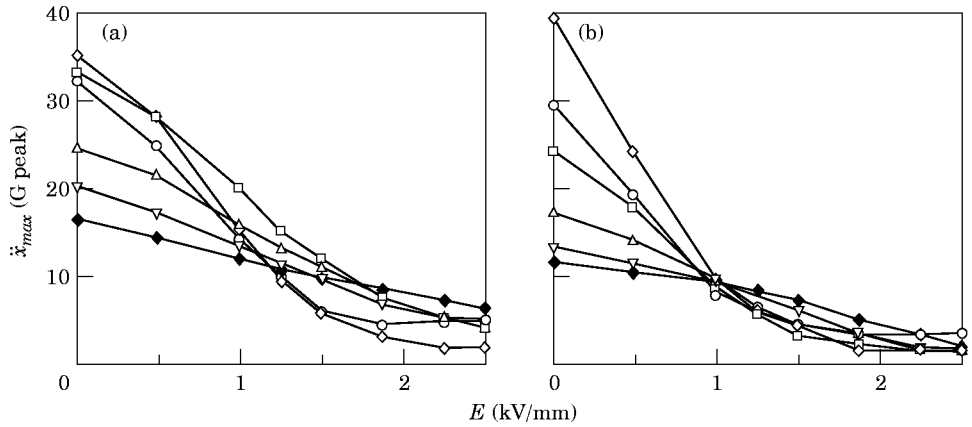

Figure 3. Maximum acceleration versus Electric field intensity for (a) MP damper and (b) SP damper. Frequencies (Hz): –○–, 10; –◇–, 20; –□–, 30; –△–, 40; –▽–, 50; –◆–, 60.

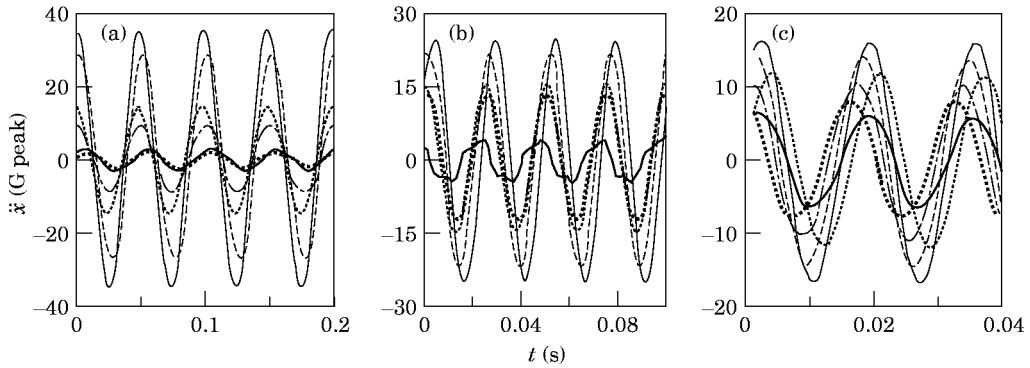

Figure 4. Acceleration of the MP ER damper (experimental) for (a) 20 Hz, (b) 40 Hz and (c) 60 Hz. Electric field intensities (kV/mm): ——, 0·0, - - - - -, 0·5; ····, 1·0; ·–·–·–, 1·25; ·····, 1·875; ——, 2·5.

friction force. Large viscous damping can suppress vibration in lower frequencies whereas large Coulomb friction force will enhance vibration in higher frequencies. Similar phenomena are also found in swept random experiments. Figure 3(b) shows the variation of maximum accelerations of the SP damper varying with the electric field intensity for different excitation frequencies. Similar conclusions can be obtained from Figure 3(a). The accelerations of the SP damper increase with the increasing of electric field intensity for frequenices greater than 100 Hz, which is similar to that of the MP damper.

The experimental results of acceleration for the MP damper are shown in Figure 4, for the excitation frequencies of 20, 40 and 60 Hz respectively and the electric field intensity changing from 0–2.5 kV/mm. The strength of the excitation force is also different for different frequencies. At low frequencies (20, 40 Hz), the damper is very effective in vibration control when the electric field intensity changes from 1 to 1·875 kV/mm. The ER damper exhibits non-linearity in high electric field intensity. Due to the non-linearity of ER fluid, the higher the intensity of the electric field, the stronger the nonlinear effect will be. The characteristics of ER fluid depend on electric field intensity and shear rate etc., so the non-linearity of the ER damper depends on the excitation frequency and the electric field intensity etc. Similar results for the SP damper for different frequencies and different electric field intensities are given in Figure 5. Similar conclusions can be obtained.

When the electric field intensity changes from 0 to 2.5 kV/mm, the swept random experiments are carried out for each of these two dampers to show the characteristics of

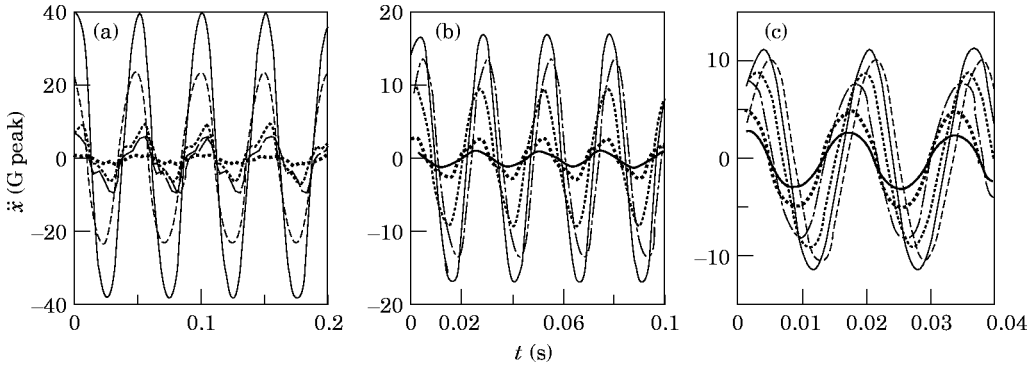

Figure 5. Acceleration of the SP ER damper (experimental) for (a) 20 Hz (b) 40 Hz and (c) 60 Hz. Key for field intensities as for Figure 4.

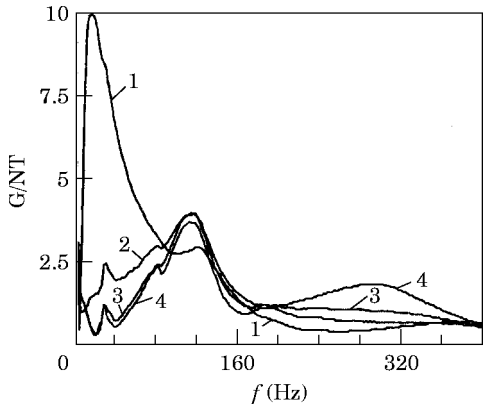

Figure 6. Swept random test results for the MP damper. Electric field intensities (kV/mm): 1, 0·0; 2, 0·5; 3, 1·5 and 4, 2·25.

the ER dampers at different frequencies. Figures 6 and 7 show the transfer functions of these two dampers. For the MP damper, when the electric field intensity is 0.5 kV/mm, the amplitude of the transfer function in the lower frequency bands is suppressed and peaks appear at 30 and 118 Hz. The increase in amplitude for frequencies higher than 100 Hz is consistent with the results in sinusoidal excitations. Roughly speaking, the MP damper can only suppress the response in lower frequeny bands. In Figure 7 for the SP damper, there is a peak around 120 Hz. The damping effect of the SP damper can be clearly seen within the frequency band, 0–120 Hz. The phenomenon may be explained as follows: The damping increases with the increase in electric field intensity, and heavy damping is very effective for reducing vibration in the lower frequency bands. On the other hand, when the electric field intensity is over a threshold value, the Coulomb friction force becomes predominant. Above the threshold value, the responses increase with the increase in the Coulomb friction force in the higher frequency band. The natural frequencies of both dampers shift to higher frequencies due to an increase in stiffness. The varying damping range of the MP damper is broader than that of the SP damper.

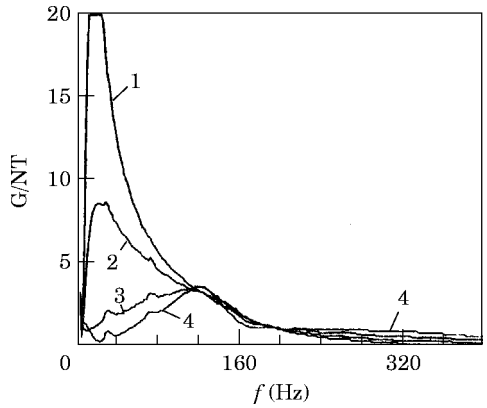

Figure 7. Swept random test results for the SP damper. Key for field intensities for Figure 6.

4. ESTIMATION OF ER DAMPER PARAMETERS

ER fluid will change from liquid to a solid-like structure over threshold electric field intensity and exhibit solid-like characteristics. The damping is composed of a viscous friction term and a Coulomb friction term (dry friction force). Both friction forces must be considered in parameters estimation, as both of them depend on the electric field intensity. The damper, in an experiment, can be assumed to be a single-degree-of-freedom system. Then the differential equation of the system can be obtained as:

$$m\ddot{x} + c_v\dot{x} + kx + c_c \operatorname{sgn}(\dot{x}) = F \sin \omega t \tag{1}$$

where m, c_v, c_c and k are the mass (kg), viscous friction coefficient (Ns/m), Coulomb friction (N) and stiffness (N/m), respectively. F is the amplitude of excitation force (N) and ω is the angular frequency of sinusoidal excitation (rad/s).

For simplicity, Equation (1) is non-dimensionalized by dividing by $me\omega^2$ on both sides, where e is a reference displacement (mm). In this paper $e = 1$ (mm), so that

$$\ddot{\bar{x}} + \bar{c}_v\dot{\bar{x}} + \bar{k}\bar{x} + \bar{c}_c \operatorname{sgn}(\dot{\bar{x}}) = \bar{F} \sin \tau \tag{2}$$

where $\bar{c}_v = c_v/m\omega$, $\bar{k} = k/m\omega^2$, $\bar{c}_c = c_c/me\omega^2$, $\bar{F} = F/me\omega^2$, $\bar{x} = x/e$ and $\tau = \omega t$. The displacement x is replaced by dimensionless $\bar{x}$. The unknown parameters ($\bar{c}_v$ and $\bar{c}_c$) in equation (2) can be defined as additional state variables by introducing state transformation:

$$x_1 = \bar{x}, \qquad x_2 = \dot{\bar{x}}, \qquad x_3 = \bar{c}_c, \qquad x_4 = \bar{c}_v \tag{3}$$

Equation (2) can be written in matrix form:

$$\dot{\mathbf{X}} = \mathbf{f}(\mathbf{X}, \tau) \tag{4}$$

where $\mathbf{X} = [x_1 \quad x_2 \quad x_3 \quad x_4]^{\mathrm{T}}$, and

$$\mathbf{f}(\mathbf{X}, \tau) = \begin{bmatrix} x_2 \\ -\bar{k}x_1 - x_3 \operatorname{sgn}(x_2) - x_4x_2 + \bar{F} \sin \tau \\ 0 \\ 0 \end{bmatrix} \tag{5}$$

The displacement response is obtained through numerical integration of the acceleration response, and the non-dimensionless displacement response is considered as an available observation of the system. According to the algorithm in Reference [15], the state estimation can be obtained by a recursive least-square algorithm. Estimation of $\hat{\mathbf{X}}$ can be provided by a predictor–corrector expression:

$$\dot{\hat{\mathbf{X}}} = \mathbf{f}(\hat{\mathbf{X}}, \tau) + 2\mathbf{PHQ}\{\mathbf{Z}(\tau) - \mathbf{h}(\hat{\mathbf{X}}, \tau)\} \tag{6}$$

where $\mathbf{f}(\hat{\mathbf{X}}, \tau)$ can be obtained from equation (5), and $\mathbf{Z}(\tau)$ is expressed as follows:

$$\mathbf{Z}(\tau) = \mathbf{h}(\mathbf{X}, \tau) + \text{observation noise} \tag{7}$$

where $\mathbf{h}(\mathbf{X}, \tau)$ is a real value, $\mathbf{h}(\mathbf{X}, \tau) = x_1$, since in this paper there is only a single observation. $\mathbf{h}(\hat{\mathbf{X}}, \tau)$ is the estimation of x_1.

The error residuals $\{\mathbf{Z}(\tau) - \mathbf{h}(\hat{\mathbf{X}}, \tau)\}$ are weighted by a matrix of three terms: an error covariance matrix $\mathbf{P}$ of dimension (4×4); a matrix $\mathbf{H}$ where $\mathbf{H} \triangleq \partial\mathbf{h}(\hat{\mathbf{X}}, \tau)/\partial\hat{\mathbf{X}} = [1 \quad 0 \quad 0 \quad 0]^{\mathrm{T}}$; a weighting matrix $\mathbf{Q}$ for a single observation, which reduces to a scalar and can be taken as 1.

The next stage is to update the elements of **P** for each recursive step. This is obtained from the solution of the equations:

$$\frac{\mathrm{d}\mathbf{P}}{\mathrm{d}\tau} = \frac{\partial \mathbf{h}(\hat{\mathbf{X}}, \tau)}{\partial \hat{\mathbf{X}}}\mathbf{P} + \mathbf{P}\frac{\partial \mathbf{f}^{\mathrm{T}}(\mathbf{X}, \tau)}{\partial \hat{\mathbf{X}}} + 2\mathbf{P}\frac{\partial}{\partial \hat{\mathbf{X}}}[\mathbf{HQ}\{\mathbf{Z}(\tau) - \mathbf{h}(\hat{\mathbf{X}}, \tau)\}]\mathbf{P} \tag{8}$$

The solution of equation (8) requires the pre-computation of the Jacobian matrix.

$$\frac{\partial \mathbf{h}(\hat{\mathbf{X}}, \tau)}{\partial \hat{\mathbf{X}}} = \begin{bmatrix} 0 & 1 & 0 & 0 \\ -\bar{k} & -\hat{x}_4 & -\mathrm{sgn}\,(\hat{x}_2) & -\hat{x}_2 \\ 0 & 0 & 0 & 0 \\ 0 & 0 & 0 & 0 \end{bmatrix}$$

which demonstrates that **P** is a function of the evolving state estimation $\hat{\mathbf{X}}$. The initial values of $\bar{c}_v$ and $\bar{c}_c$ can be taken as zero, while the initial value of x_1 and x_2 can be obtained through numerical integration of the acceleration. Matrix **P** is taken as:

$$\mathbf{P} = \begin{bmatrix} 4 & 1 & 1 & 1 \\ 1 & 4 & 1 & 1 \\ 1 & 1 & 4 & 1 \\ 1 & 1 & 1 & 4 \end{bmatrix}$$

State variables can be obtained by solving equations (6) and (8) with the fourth order Runge–Kutta integration algorithm. First, equation (6) is integrated one step using the initial values with the Runge–Kutta integration algorithm. Then the Jacobian matrix is obtained. Finally the matrix **P** is updated by integrating the equation. In each recursion of the matrix **P**, the error between estimation and observation becomes smaller and smaller. The recursion continues until the error is within the given limit. So the estimation of responses, viscous friction coefficient and Coulomb friction coefficient can be finally obtained.

In Reference [14], the recursive least-square algorithm was used to estimate parameters of the ER damper too, but the authors had not considered the change in stiffness with electric field intensity. From the experiments, it can be seen clearly that not only the damping, but also the stiffness changes with electric field intensity, and so the viscous friction coefficient, Coulomb friction force and stiffness must be included in the estimation. When the electric field intensity is lower than 1·25 kV/mm, the estimation of Coulomb friction force is negative or the state variables are unstable, and the algorithm is no longer applicable. The parameters for excitation frequencies 10, 20 and 30 Hz are estimated through experimental data. Stiffness, viscous friction coefficient and Coulomb friction are shown in Figure 8, for the electric field intensity changing from 1·25 to 2·5 kV/mm. The stiffness increases sharply compared with those obtained without the electric field case (the stiffness is about 750 N/m without electric field). The changing rate of stiffness depends on the excitation frequency. For electric field intensities between 1·25 and 2·5 kV/mm, the stiffness has no obvious change at 10 Hz, but it changes obviously at 20 Hz. The viscous friction force increases slowly at 10 Hz and decreases at 20 and 30 Hz, while Coulomb friction increases at all these three frequencies. The above mentioned phenomena can be explained as follows. When the electric field intensity is below a threshold value, ER fluid is still in its liquid state and exhibits the liquid characteristics. In this state, the Coulomb friction force is not operative and is very small, while viscous friction increases rapidly with the increase in electric field intensity and plays the dominant role. When the electric field

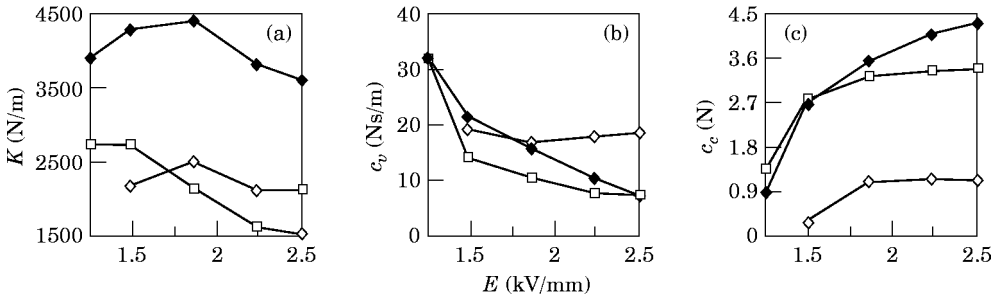

Figure 8. Variation of estimated MP damper parameters versus electric field intensity for (a) Stiffness, (b) Viscous friction coefficient and (c) Coulomb friction coefficient. Frequencies (Hz); –◇–, 10; –□–, 20; –◆–, 30.

intensity is over a threshold value, ER fluid loses its liquid characteristics and exhibits solid-like characteristics. Then the Coulomb friction force becomes predominant, which leads to the amplification of response. For the excitation at 10 Hz and the electric field intensity at 1·5 kV/mm, the estimated and experimental results of responses, viscous friction coefficient and Coulomb friction are shown in Figure 9. From Figure 9, one can see that when the recursion is over 1200 steps, the estimation of response converges to that of the experiment. When the recursion is over 2000 steps, the viscous friction coefficient and Coulomb friction converge to constants. The recursive least-square algorithm is unsuitable for the SP damper owing to its small viscous friction and Coulomb friction.

5. CONCLUSIONS

From experiments and estimation, the following conclusions can be obtained for these ER dampers:

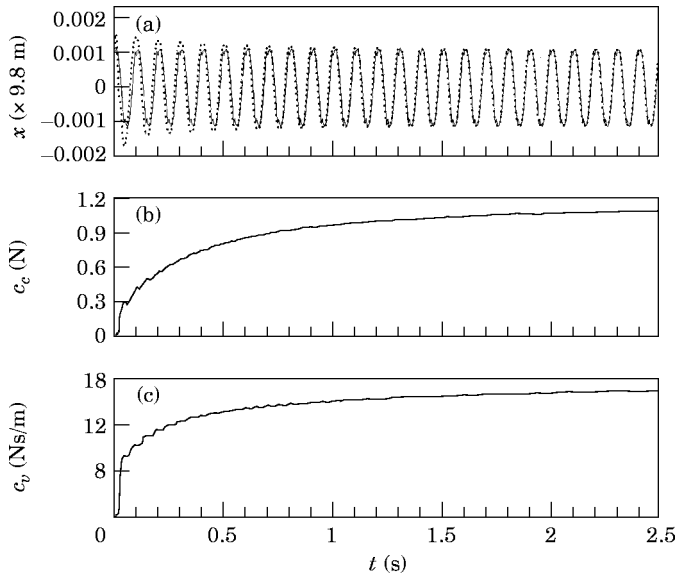

Figure 9. Estimated response and damping of MP damper. (a) Comparison of estimated (····) and experimental (——) results; (b) Coulomb friction and (c) viscous friction coefficient.

(1) Both ER dampers are very effective in vibration control, when the frequency is below 100 Hz. These two ER dampers are less or no longer effective for excitation frequencies over 100 Hz.

(2) When the electric field intensity is over a threshold value, these two ER dampers exhibit strong non-linearity, depending also on the excitation frequency. The lower the frequencies and the higher the electric field intensities are, the stronger the non-linear effect will be.

(3) Each of these two ER dampers shifts its natural frequency due to the change in stiffness. Large viscous damping of the ER damper will suppress the response in the low frequency band, while a Coulomb friction will have a larger effect on the response in the high frequency band.

(4) By considering the change in stiffness, the estimated response agrees with the experimental response very well. Under lower electric field intensity, the effect of viscous friction is predominant, while under higher electric field intensity the effect of Coulomb friction is predominant.

(5) In the experiments, one finds that the varying damping range of the MP damper is broader than that of the SP damper. The MP damper seems to be more effective in vibration control.

ACKNOWLEDGMENTS

The supports of the Natural Science Foundation and the Aeronautic Science Foundation of China are greatly acknowledged. The help from M. Xu, J. R. Xu, Z. Y. Yuan, C. H. Fan and J. C. Zhen is appreciated.

REFERENCES

1. F. E. Filisko 1992 *Proceeding of the Third International Symposium on ER Fluids* (Editor R. Tao). Singapore: World Scientific, 116–128. Rheological properties and models of dry ER material.
2. H. Block, P. Rattery and T. Watson 1992 *Proceedings of the Third International Symposium on ER Fluids* (Editor R. Tao). Singapore: World Scientific, 93–115. Semi-conducting polymers as ER fluids substrate.
3. T. Hao, Y. H. Chen, M. Xu and Y. Z. Xu 1994 *Chinese Advances in Mechanics* **24**, 315–335. Research advances of electro-rheology (in Chinese).
4. N. K. Petek 1992 *Society of Automotive Engineers* 920275. An electronically controlled shock absorber using electro-rheological fluid.
5. S. Morishita and J. Mitsui 1991 *Society of Automotive Engineers* 910744. Controllable shock absorber system (an application of electro-rheological fluid).
6. X. M. Wu, R. Stanway and J. L. Sproston 1990 22*nd International Symposium on Automation Technology and Automation*, *Florence*, 14–18 May. ISATA Proceedings 2, Croyden 823–830. Electro-rheological fluids and their application in active suspension and power transmission.
7. A. D. Dimarogonas and A. Kollias 1992 *STLE Journal of Tribology Transactions* **35**, 611–618. Electro-rheological fluid-controlled "smart" journal bearing.
8. J. Tichy 1993 *STLE Journal of Tribology Transactions* **36**, 127–133. Behavior of a squeeze film damper with an electro-rheological fluid.
9. A. Kollias and A. D. Dimarogonas 1993 *Third International Conference on Adaptive Structures*. Technomic Publishing Company, 176–193. Damping of rotor vibration using electro-rheological fluids in disc type devices.
10. G. Meng, D. Z. Ying and G. Z. Yao 1996 *Journal of Aerospace Power* **11**, 265–278. Experimental investigation on rotor vibration control by electro-rheological damper (in Chinese).
11. T. C. Jordan and M. T. Shaw 1989 *IEEE Transactions on Electrical Insulation* **24**, 849–878. Electro-rheology.

12. G. Z. Yao, G. Meng and T. Fang 1995 *Journal of Machine Vibration* **4**, 232–240. The characteristics research of electro-rheological fluid and its application for vibration control.
13. T. G. Duclos 1988 *Society of Automotive Engineers* 881134. Design of devices using electro-rheological fluids.
14. D. M. Detchmendy and R. Sridhar 1966 *Transactions of ASME*, *Journal of Basic Engineering* **88**, 362–368. Sequential estimation of combined of states and parameters in noisy non-linear dynamics systems.
15. R. Stanway, J. L. Sproston and N. G. Stevens 1987 *Journal of Electrostatics* **20**, 167–184. Non-linear modelling of an electro-rheological vibration damper.